Crystal Structures of Apo and Metal-Bound Forms of the UreE Protein from Helicobacter pylori: Role of Multiple Metal Binding Sites

ARTICLE *in* BIOCHEMISTRY · AUGUST 2010

Impact Factor: 3.02 · DOI: 10.1021/bi100372h · Source: PubMed

8 AUTHORS, INCLUDING:

Stéphane L Benoit
University of Georgia
29 PUBLICATIONS **609** CITATIONS
SEE PROFILE

Erica F Miller-Parks
Contra Costa College
6 PUBLICATIONS **45** CITATIONS
SEE PROFILE

Robert J Maier
University of Georgia
195 PUBLICATIONS **5,532** CITATIONS
SEE PROFILE

7080 *Biochemistry* **2010,** *49,* 7080–7088
DOI: 10.1021/bi100372h

BIOCHEMISTRY
including biophysical chemistry & molecular biology
Article

Crystal Structures of Apo and Metal-Bound Forms of the UreE Protein from *Helicobacter pylori*: Role of Multiple Metal Binding Sites[†,‡]

Rong Shi,[§] Christine Munger,[§] Abdalin Asinas,[§,@] Stéphane L. Benoit,[∥] Erica Miller,[∥] Allan Matte,[⊥] Robert J. Maier,*[,∥] and Miroslaw Cygler*[,§,⊥]

[§]*Department of Biochemistry, McGill University, Montreal, Québec, Canada H3G 1Y6,* [∥]*Department of Microbiology, University of Georgia, Athens, Georgia 30602, and* [⊥]*Biotechnology Research Institute, 6100 Royalmount Avenue, Montreal, Québec, Canada H4P 2R2.* [@]*Current address: The Structural Genomics Consortium, University of Toronto, Toronto, Ontario, Canada.*

Received March 10, 2010; Revised Manuscript Received July 15, 2010

ABSTRACT: The crystal structure of the urease maturation protein UreE from *Helicobacter pylori* has been determined in its apo form at 2.1 Å resolution, bound to Cu^{2+} at 2.7 Å resolution, and bound to Ni^{2+} at 3.1 Å resolution. Apo UreE forms dimers, while the metal-bound enzymes are arranged as tetramers that consist of a dimer of dimers associated around the metal ion through coordination by His102 residues from each subunit of the tetramer. Comparison of independent subunits from different crystal forms indicates changes in the relative arrangement of the N- and C-terminal domains in response to metal binding. The improved ability of engineered versions of UreE containing hexahistidine sequences at either the N-terminal or C-terminal end to provide Ni^{2+} for the final metal sink (urease) is eliminated in the H102A version. Therefore, the ability of the improved Ni^{2+}-binding versions to deliver more nickel is likely an effect of an increased local concentration of metal ions that can rapidly replenish transferred ions bound to His102.

The enzyme urease catalyzes hydrolysis of urea to ammonia and carbamate. While most bacterial ureases are composed of three different subunits that form a $(UreABC)_3$ structure, *Helicobacter pylori* urease has only two subunits, UreA and UreB, organized as a $[(ureAB)_3]_4$ complex (for a recent review, see ref *1*). Urease is dependent on the presence of two bound Ni^{2+} ions per UreB subunit for its activity (*1*). Insertion of the Ni^{2+} ions into urease requires a series of maturation proteins that have been best-studied in *Klebsiella aerogenes*, including UreD (UreH in *H. pylori*), UreE, UreF, and UreG (*2*). Interactions between the urease apoprotein subunits and maturation proteins, as well as interactions among the maturation proteins themselves, have been identified by various approaches in *K. aerogenes* (reviewed in ref *1*), *Proteus mirabilis* (*3*), and *H. pylori* (*4*−*6*). Although the specific molecular roles of each of the accessory proteins in metal center maturation and the requirements for protein−protein interactions are not clear, the overall conclusion from studies of *K. aerogenes* is that UreD, UreF, and UreG form a complex with the urease apoprotein while UreE functions in Ni^{2+} delivery. In *H. pylori*, using tandem affinity purification and either UreA, UreB, or UreG as bait, Stingl and co-workers revealed the following interactions: UreA with UreB, UreA with UreH, UreE with UreG, and UreF with UreH (*6*); the UreE−UreG interaction has also been reported by two other groups (*4*, *5*).

[NiFe] hydrogenases also require several maturation proteins for assembly of the [NiFe] cluster, and it has been found that the urease and hydrogenase maturation systems in the gastric pathogen *H. pylori* share some accessory proteins (*7*−*9*). For example, an interaction between *H. pylori* UreE and HypA, the latter protein being a component of the [NiFe] hydrogenase maturation pathway, has been shown to be necessary for urease maturation (*9*). Similarly, *H. pylori* UreG can interact with another hydrogenase maturation protein, HypB (*6*).

The UreE protein appears to function as a nickel metallochaperone, acting as the source of Ni^{2+} ions for urease, with His96 of *K. aerogenes* (*Ka*UreE),[1] the equivalent of His100 of *Bacillus pasteurii* (*Bp*UreE) and His102 of *H. pylori* (*Hp*UreE) postulated to play a role in Ni^{2+} transfer (*4*, *10*−*12*). The numbers of Ni^{2+} ions bound per UreE dimer range from one for *Hp*UreE (*4*, *13*) to six for *Ka*UreE (*14*). *Bp*UreE binds two Ni^{2+} ions per dimer under physiological conditions (*15*). In many microorganisms (including *K. aerogenes, P. mirabilis*, or *Pseudomonas aeruginosa*), the UreE proteins contain C-terminal sequences rich in histidines (*16*) that have been shown to confer additional Ni^{2+} binding capacity. Upon addition of His tag motifs to the C-terminus of the *Hp*UreE, it was possible to enhance the Ni binding capacity of the protein (*13*). As a consequence, the urease activity increased, indicating a link between the Ni binding ability of UreE and urease activity in vivo (*13*).

The metal binding properties of *Bp*UreE, *Ka*UreE, and *Hp*UreE have been investigated in detail, revealing different thermodynamic properties for metal binding by the three proteins (*4*, *11*, *14*, *17*). In addition to binding Ni^{2+}, these proteins can also bind zinc (Zn^{2+}), cobalt (Co^{2+}), and copper (Cu^{2+}).

[†]This work was supported up an operating grant (GSP-48370) from the Canadian Institutes for Health Research to M.C. and A.M. and by the Georgia Foundation (endowment for R.J.M.).

[‡]Coordinates and structure factors have been deposited in the Protein Data Bank as entries 3L9Z, 3NXZ, 3NY0, and 3LA0.

*To whom correspondence should be addressed. R.J.M.: Department of Microbiology, University of Georgia, Athens, GA 30602; telephone, (706) 542-2323; fax, (706) 542-2674; e-mail, rmaier@uga.edu. M.C.: Biotechnology Research Institute, 6100 Royalmount Ave., Montreal, QC, Canada H4P 2R2; telephone, (514) 496-6321; fax, (514) 496-5143; e-mail, mirek@bri.nrc.ca.

[1]Abbreviations: *Hp*UreE, *H. pylori* UreE; *Bp*UreE, *B. pasteurii* UreE; *Ka*UreE, *K. aerogenes* UreE.

 Published on Web 07/15/2010

Table 1: Oligonucleotide Primers Used in This Study

primer name	sequence[a] (5′ → 3′)	restriction endonuclease sites
UPHPUreE	CCGGCAGCCATATGATCATAGAGCGTTTAAT	*Nde*I
RevSTOPUreE	CAGGTGAGTCGACCCTTTATCCATTTG	*Sal*I
RevGOPUreE	GACGGCGGTCGACTTTCATGACCACTTTAAA	*Sal*I
H102A Rev	GAAATAGGAAACCGC**GCT**GCGGCTTTATACTATGGC	
H102A Fwd	CGCCATAGTATAAAGCCGC**AGC**GCGGTTTCCTATTTC	
F28D Fwd	CGAGCGATCTTCTTCCTCGTT**TCA**TCCCATTCTAAATCC	
F28D Rev	GGATTTAGAATGG**GAT**GAAACGAGGAAGAAGATCGCTCG	
NHis UreE Fwd	CCGGCACATATGCACCACCACCACCACCACATCATAGAGCGTTTAGTTGGC	*Nde*I
Cm2	AATGGGTTATCTCGGCGGTCACTC	

[a]Bold letters indicate sites of mutagenesis. Underlined regions indicate engineered restriction sites.

Purified *Bp*UreE has been shown to contain one Zn^{2+} per dimer, but with dimer formation being independent of Zn^{2+} binding (*17*). Metal binding studies of *Bp*UreE by EXAFS and inductively coupled plasma-optical emission spectrometry (ICP-OES) produced two possible models for nickel binding (*15*). One model invokes two identical Ni^{2+} binding sites in which each metal ion binds His100 and either His145 or His147 of the same monomer, while the alternative model involves two different binding sites with different Ni^{2+} affinities. The latter model would also involve His100 as a Ni^{2+}-binding site but requires that two His100 residues from different monomers would together coordinate one Ni^{2+} ion, whereas the other Ni^{2+} ion is bound by a pair of histidines, either His145 or His147. Interestingly, in *Ka*UreE, the best fit to the ITC data is with a model that assumes that the C-terminal His-rich tail binds Ni^{2+} ions more weakly than the rest of the protein dimer, which binds the first two Ni^{2+} ions in a manner independent of the His-rich tail (*14*). A recent report suggests that *Hp*UreE can also bind Zn^{2+} and that mutation of the conserved His102 results in the loss of Ni^{2+} and Zn^{2+} binding by the protein (*4*). Here we address the question of the role of the His-rich regions in delivering Ni^{2+} to the penultimate acceptor protein, urease.

Previously, the crystal structures of UreE have been determined for *Ka*UreE (*18*) and *Bp*UreE (*19*), and the solution structure of the latter has also been investigated by NMR (*20*). The crystal structure of *Bp*UreE reveals tetramers formed as a dimer of dimers, with each of the four His100 residues contributing to the coordination of the Zn^{2+} ion (*19*). *Ka*UreE crystallized as dimers with and without Cu^{2+} ions. One of the Cu^{2+} ions is coordinated by His96 (equivalent to His100 in *BpUreE*) from two molecules of the dimer. In this study, we report the crystal structure of *Hp*UreE in apo and metal-bound forms and show that, under our crystallization conditions, the presence of metal ions promotes tetramer formation. The contacts between the dimers within a tetramer are limited to the metal coordination by His102 residues and van der Waals interactions between Phe28 and its counterpart. While UreE can bind several nickel ions, we propose that only the Ni^{2+} ion that is coordinated by His102 (or its equivalent in related proteins) can be transferred to the apo-urease acceptor. Our results with *Hp*UreE engineered to have a His tag at either the N- or C-terminus indicate that the His-rich segments present in some UreE proteins augment Ni sequestering abilities and urease activation, likely by more efficient metal transfer to His102. This is probably due to an increased local concentration of metal ions available for binding to the biologically essential site rather than direct transfer without the participation of His102.

MATERIALS AND METHODS

Bacterial Strains and Growth Conditions. *Escherichia coli* DH5α was used for all cloning steps. *H. pylori* strain ATCC 43504 was used as the wild-type for in vivo studies of *ureE* site-directed mutants. *E. coli* was grown in Luria-Bertani medium supplemented with 100 μg/mL ampicillin or 30 μg/mL chloramphenicol, as required. *H. pylori* was grown on Brucella agar plates supplemented with 10% defibrinated sheep blood (BA plates) and 30 μg/mL chloramphenicol and/or 25 μg/mL kanamycin as required.

Construction of Plasmids Used for Insertion of ureE Variants into the H. pylori Chromosome. Site-directed mutagenesis of *ureE* was conducted using overlap extension PCR (*21*). *ureE* gene was amplified in two parts using either Platinum*Pfx* (Invitrogen) or iProof (BioRad) high-fidelity polymerase. Genomic DNA was used as a template, along with the appropriate primers to impart the desired mutation (Table 1). The final 0.5 kb PCR product was digested with *Nde*I and *Sal*I and ligated into an identically digested pPA plasmid. Each *ureE* variant was then released from the plasmid via digestion with *Bgl*II and *Sal*I (with the exception of pPA-HPH6, which was digested with *Bgl*II and *Blp*I). In this 0.7 kb fragment, *ureAp* is directly upstream of *ureE* and can therefore drive transcription of *ureE* in *H. pylori*. This fragment was treated with *T4* DNA polymerase and ligated into pEU39cm, which had been previously digested with *Eco*RV. The final plasmid construct allowed for integration of the *ureE* variant gene into the innocuous chromosomal locus *hp0405* as previously described (*13*). The list of bacterial strains and plasmids used in this study is given in Table 2.

Construction of the Plasmid Used for Overproduction of UreE(F28D) Protein. Overlap extension PCR was used for site-directed mutagenesis of *ureE*. *H. pylori* 43504 *ureE* was amplified in two parts using genomic DNA as a template, along with the appropriate primers. The F28D primers introduce a mutation into *ureE*, resulting in an Asp instead of a Phe at position 28 of UreE. The final PCR product was digested with *Nde*I and *Sal*I and ligated into an identically digested pET21b expression vector.

Introduction of ureE Variants into H. pylori ΔureE. Plasmids pEU-HP, pEU-HP6, pEU-H6HP, pEU-H102A, pEU-H102AH6, and pEU-F28D were transformed separately into the *ureE* mutant via natural transformation. Parent *ureE* cells were grown from freezer stock on BA plates supplemented with kanamycin for 24 h and then further grown for 12 h on a fresh BA plate. Cells were then incubated for 12 h with the appropriate plasmid DNA and transferred to BA plates supplemented with chloramphenicol and kanamycin to select for recombinant

Table 2: Bacterial Strains and Plasmids Used in This Study

strain or plasmid	characteristics[a]	source or reference
	Strains	
H. pylori 43504	parent strain	ATCC
ureE mutant	Δ*ureE::aphA3* Kan^r	*5*
ureE [UreE]	Δ*ureE hp0405::*Φ (*ureAp-ureE-cat*) Cm^r Kan^r	this study
ureE [UreE-H6]	Δ*ureE hp0405::*Φ (*ureAp-ureE* $[His]_6$-*cat*) Cm^r Kan^r	this study
ureE [H6-UreE]	Δ*ureE hp0405::*Φ (*ureAp*-$[His]_6$*ureE-cat*) Cm^r Kan^r	this study
ureE [UreE(H102A)]	Δ*ureE hp0405::*Φ (*ureAp-ureE*(*H*→*A*)-*cat*) Cm^r Kan^r	this study
ureE [UreE(H102A)-H6]	Δ*ureE hp0405::*Φ (*ureAp-ureE*(*H*→*A*)[His_6]-*cat*) Cm^r Kan^r	this study
ureE [UreE(F28D)]	Δ*ureEhp0405::*Φ(*ureAp-ureE*(*F*→*D*)-*cat*) $Cm^r Kan^r$	this study
E. coli		
DH5α	cloning strain	
	Plasmids	
pPA	pET21b derivative in which *ureAp* (*ureA* promoter region) replaces *T7p* to promote gene expression in *H. pylori*, Amp^r	*13*
pEU39cm	suicide vector used for homologous recombination into *hp0405*, Ap^r Cm^r	*7*
pPA-HP	*H. pylori ureE* cloned into pPA	*13*
pPA-HPH6	*H. pylori ureE* (no stop codon) cloned into pPA	*13*
pPA-H6HP	*H. pylori ureE* with six upstream histidine codons cloned into pPA	this study
pPA-H102A	*H. pylori ureE* variant (mutated gene encoding His102Ala) cloned into pPA	this study
pPA-H102AH6	*H. pylori ureE* variant (mutated gene encoding His102Ala and lacking a stop codon) cloned into pPA	this study
pPA-F28D	*H. pylori ureE* variant (mutated gene encoding Phe28Asp) cloned into pPA	this study
pEU-HP	*Bgl*II/*Sal*I fragment of pPA-HP (encoding UreE) cloned into pEU39cm	*13*
pEU-HPH6	*Bgl*II/*Blp*I fragment of pPA-HP6 (encoding UreE-His_6) cloned into pEU39cm	*13*
pEU-H6HP	*Bgl*II/*Sal*I fragment of pPA-H6HP (encoding His_6-UreE) cloned into pEU39cm	this study
pEU-H102A	*Bgl*II/*Sal*I fragment of pPA-H102A [encoding UreE(H102A)] cloned into pEU39cm	this study
pEU-H102AH6	*Bgl*II/*Sal*I fragment of pPA-H102AH6 [encoding UreE(H102A)-His_6] cloned into pEU39cm	this study
pEU-F28D	*Bgl*II/*Sal*I fragment of pPA-F28D [encoding UreE(F28D)] cloned into pEU39cm	this study

[a] *hp* refers to the locus in the *H. pylori* ATCC 26695 genome.

strains containing the variant *ureE* at the *hp0405* locus. Mutants were confirmed by sequencing using the Cm2 primer (University of Georgia Sequencing and Synthesis Facility, Athens, GA).

Urease Assay. *H. pylori* cell-free extracts (CFE) were assayed for urease activity. *H. pylori* strains were grown for 24 h on BA plates, resuspended in 50 mM HEPES-NaOH (pH 7.5), washed once with the same buffer, and then sonicated. Cell debris was removed by centrifugation for 10 min at 10000*g*. The protein concentration was measured using the BCA protein assay kit (Thermo Fisher scientific), and the CFE was diluted to a protein concentration of 100 μg/mL. One microgram of CFE protein was incubated for 10 min at 37 °C in HEPES buffer with 30 mM urea. The amount of ammonia released from urea hydrolysis was measured using the phenol-hypochlorite assay (*22*). Serial dilutions of NH_4Cl were used to create a standard curve to convert the absorbance at 625 nm to nanomoles of ammonia. Urease activity is defined as the number of micromoles of ammonia produced per minute per milligram of total protein. Results shown are averages and standard deviations from assays conducted in triplicate for one growth experiment. The same patterns were seen for two additional (independent) growth experiments.

Immunoblotting. Anti-UreE antibodies were used to compare levels of UreE protein expression among the strains of *H. pylori* (*13*). Ten micrograms of each CFE was separated using sodium dodecyl sulfate−12.5% polyacrylamide gel electrophoresis (SDS−PAGE) alongside prestained molecular weight markers (Bio-Rad). Proteins were then transferred to a nitrocellulose membrane (0.45 μm pore size, GE Water & Process Technologies) as previously described (*23*). Following transfer, the membrane was blocked overnight with 3% (w/v) gelatin prepared in 20 mM Tris-HCl (pH 7.6) and 100 mM NaCl (TBS). The membrane was washed briefly with 0.1% (v/v) Tween 20 in TBS (TTBS) followed by a 2 h incubation with anti-UreE (1:500 dilution) at room temperature in TTBS with 1% (w/v) gelatin. The secondary antibody incubation was performed in a similar manner using goat anti-rabbit IgG (H+L)−AP conjugate (Bio-Rad, 1:1000 dilution). Following each antibody incubation, the membrane was washed three times in 100 mL of TTBS. UreE-specific bands were visualized using 5-bromo-4-chloro-3′-indolyl phosphate (BCIP) and Nitro-Blue Tetrazolium (NBT) as previously described (*24*).

Expression and Purification of UreE and UreE(*F28D*). *E. coli* BL21(DE3) Rosetta cells (Novagen) harboring either plasmid pET-UreE (*13*) or plasmid pET-UreE F28D were grown in 1 L of terrific broth (TB) containing 100 μg/mL ampicillin and 34 μg/mL chloramphenicol. Cells were cultured at 37 °C until the OD_{600} was approximately 0.6; isopropyl β-D-galactopyranoside (IPTG) was added to a final concentration of 500 μM, and cells were cultured overnight at 20 °C. Cells were harvested by centrifugation (4000*g* for 30 min at 4 °C). Cells were resuspended in a buffer consisting of 20 mM HEPES (pH 7.5) and 5% (v/v) glycerol and lysed on ice by sonication using alternating cycles of 15 s on and 15 s off for a total of 2 min. Following sonication, the protease inhibitors benzamidine and leupeptin at final concentrations of 0.5 mM and 10 μM, respectively, were added to the lysate. The lysate was clarified by centrifugation (34000*g* for 1 h at 4 °C) and the protein supernatant applied to a 5 mL bed volume HiTrap SP cation exchange column mounted on an AKTA purifier FPLC system (GE Healthcare), with the column equilibrated in 20 mM HEPES buffer (pH 7.5). Following

washing using the same buffer until the A_{280} reached baseline, proteins were eluted via application of a NaCl gradient, with UreE eluting at ~300 mM NaCl. Fractions containing UreE as assessed by SDS−PAGE were pooled and loaded on a Superdex 75 column equilibrated in 20 mM HEPES buffer (pH 7.5) and 100 mM NaCl. The protein ran as a doublet by SDS−PAGE and gave apparent masses of 18335 and 18149 Da (expected value of 19381.5 Da) when analyzed by ESI-TOF MS (Waters). However, addition of protease inhibitor cocktail (Sigma) prevented this proteolysis. UreE was concentrated to 12 mg/mL by ultrafiltration in a final buffer of 20 mM HEPES (pH 7.5) and 100 mM NaCl prior to crystallization. In several crystallization trials, we have mixed UreE with either HypA or UreG. HypA was expressed and purified as described previously (*25*). UreG with a C-terminal His tag was copurified with UreE (no tag) through Ni-NTA affinity purification. In brief, pellets were resuspended in a buffer containing 20 mM HEPES (pH 7.5), 100 mM NaCl, and 0.1 mM TCEP and lysed on ice by sonication using alternating cycles of 15 s on and 15 s off for a total of 2 min. Following sonication, the lysate was clarified by centrifugation (34000*g* for 1 h at 4 °C), and the protein supernatant of UreE and UreG were pooled prior to NiNTA binding. Elution was conducted using the buffer described above containing 250 mM imidazole. The UreE−UreG complex was separated from excess UreG on a Superdex 75 HiLoad column (GE Healthcare) in 20 mM HEPES (pH 7.5), 100 mM NaCl, and 0.1 mM TCEP. The UreE−UreG complex was concentrated to 10 mg/mL for crystallization (same buffer as gel filtration).

Crystallization. A protein sample of *Hp*UreE used for initial crystallization screening eluted as an apparent dimer from the size exclusion column. The screening was performed by sitting drop vapor diffusion in Intelliplates (Art Robbins) by mixing 0.3 μL of protein (12 mg/mL) in buffer [20 mM HEPES (pH 7.5) and 100 mM NaCl] with 0.4 μL of reservoir solution. Pro-Complex, Classic I and II, and ammonium sulfate crystallization screens (Qiagen) were used for initial screening, with several conditions yielding crystals. The best crystals of apo-UreE were obtained from a reservoir containing 0.1 M sodium citrate (pH 5.0) and 17% (w/v) PEG 8000. Apo-UreE crystals were obtained in space group $P6_422$ with one molecule in the asymmetric unit diffracting to 2.08 Å resolution and the following unit cell dimensions: $a = b = 131.0$ Å, and $c = 51.3$ Å. Next, we aimed to obtain crystals of the UreE−HypA complex and performed screening using a protein solution containing a 1:1 ratio of both proteins. The crystals appeared from a well solution containing 16% (w/v) PEG 8000, 0.1 M sodium citrate (pH 5.0), and 5% (v/v) glycerol. Silver-stained SDS−PAGE of washed crystals removed from these drops indicated that HypA was not present in the crystals, which was consistent with the solution of their crystal structures showing the presence of only UreE but with a bound metal ion. These metal−UreE crystals belong to space group $P4_12_12$ with four molecules in the asymmetric unit diffracting to 2.86 Å resolution and the following unit cell dimensions: $a = b = 85.6$ Å, and $c = 202.6$ Å . To resolve the identity of the metal, we have purified the protein again at a later time in the presence of protease inhibitor cocktail and obtained intact protein. This protein eluted from the size exclusion column in two peaks, indicating the presence of apparent dimers and tetramers. We have pooled the tetramer-containing fractions and upon rescreening obtained tetragonal crystals, in space group $P4_12_12$, from the same solution described above [16% (w/v) PEG 8000, 0.1 M sodium citrate (pH 5.0), and 5% (v/v) glycerol] but with four molecules in the asymmetric unit diffracting to 2.7 Å resolution and somewhat different unit cell dimensions: $a = b = 88.8$ Å, and $c = 203.6$ Å. We have also obtained similar *Hp*UreE crystals when attempting to cocrystallize it with UreG. Bipyramid shape crystals of UreE alone (space group $P4_12_12$; $a = b = 91.1$ Å, and $c = 202.8$ Å) were obtained from a mixture of 1 μL of protein and 1 μL of reservoir solution containing 0.1 M MES (pH 5.5) and 13% PEG 20K.

Data Collection and Structure Determination. Hexagonal crystals of *Hp*UreE were cryoprotected by being transferred to reservoir solution supplemented with 12% (v/v) ethylene glycol. X-ray diffraction data were recorded at the LRL-CAT beamline, Sector 31, Argonne National Laboratory (ANL), at 100 K using a Mar CCD 165 mm detector. Data were integrated and scaled using HKL2000 (*26*). The UreE structure was obtained by molecular replacement using Phaser from the CCP4 suite (*27*) with the search model of UreE from *B. pasteurii* (Protein Data Bank entry 1EB0). Alternating cycles of fitting with Coot (*28*) and refinement at 2.08 Å resolution using Refmac5 (*29*), including the use of TLS parameters, led to the final models. The protein forms dimers with one molecule in the asymmetric unit, and the model includes residues 1−149 and 92 waters. The C-terminus is disordered. No divalent metal ions were found in these crystals, and this structure will be termed apo-*Hp*UreE.

Tetragonal *Hp*UreE crystals grown in the presence of HypA were cryoprotected as described for the hexagonal crystal form and diffraction data collected at the LRL-CAT beamline at ANL at 100 K. Molecular replacement solution using apo-*Hp*UreE showed the presence of a dimer of dimers with a metal ion at the center, coordinated by four histidines (His102 from each monomer). The model refined at 2.86 Å resolution includes residues 1−148 in each monomer and five water molecules. On the basis of the geometry of the ligands, the metal could be Ni^{2+}, Zn^{2+}, or Cu^{2+}, but we were not able to identify this crystal unambiguously. This set is termed Me-*Hp*UreE.

To identify the metal ion, we have grown additional crystals as described above. The tetragonal crystals obtained from *Hp*UreE alone were cryoprotected as described above; the diffraction data were collected at the CMCF1 beamline at the Canadian Light Source (Saskatoon, SK), and the structure was determined by molecular replacement. These crystals diffracted to 2.7 Å resolution and contain also a dimer of dimers with a metal ion coordinated by four His102 residues. This metal ion was identified as Cu^{2+} on the basis of the fluorescence scan and by comparison of the anomalous Fourier map calculated from data collected at the copper or nickel K absorption edge. The anomalous map calculated from data collected at the copper absorption edge showed an ~30σ peak at the position of the metal ion, while that calculated from data collected at the Ni absorption edge showed only an ~5σ peak, confirming the presence of Cu^{2+} ion. There is one tetramer in the asymmetric unit in Cu-*Hp*UreE, and the model includes residues 2−149 in each monomer. Finally, the crystals obtained in the presence of UreG diffracted to 3.1 Å and, on the basis of the fluorescence scan, contained Ni^{2+} ions (Ni-*Hp*UreE). This model includes residues 2−149 in three monomers and residues 2−154 in the fourth monomer. Data collection and refinement statistics are listed in Table 3.

Coordinates and structure factors for apo-*Hp*UreE, Me-*Hp*UreE, Cu-*Hp*UreE, and Ni-*Hp*UreE have been deposited in the Protein Data Bank (PDB) as entries 3L9Z, 3LA0, 3NXZ, and 3NY0, respectively.

Table 3: X-ray Data Collection and Refinement Statistics

	apo-*Hp*UreE	Cu-*Hp*UreE	Ni-*Hp*UreE	Me-*Hp*UreE
space group	$P6_422$	$P4_12_12$	$P4_12_12$	$P4_12_12$
a, *b*, *c* (Å)	131.0, 131.0, 51.3	88.8, 88.8, 203.6	91.1, 91.1, 202.8	85.6, 85.6, 202.6
wavelength (Å)	0.9793	1.3775	1.4849	0.9793
resolution (Å)	50−2.08 (2.15−2.08)	50−2.70 (2.80−2.70)	50−3.10 (3.21−3.10)	50−2.86 (2.96−2.86)
no. of observed *hkl* reflections	251221	193939	142778	422812
no. of unique *hkl* reflections	16040	22286	14069	18190
completeness (%)	99.8 (99.5)	96.1 (65.5)	85.7 (38.9)	99.4 (97.3)
R_{sym}[a]	0.050 (0.496)	0.074 (0.458)	0.096 (0.293)	0.120 (0.347)
$I/(\sigma I)$	18.7 (2.5)	14.9 (2.9)	12.7 (5.6)	8.7 (2.2)
Wilson plot *B* (Å^2)	39.7	71.3	50.5	71.3
R_{work}[b] (no. of *hkl* reflections)	0.221 (15182)	0.256 (21050)	0.245 (13348)	0.278 (17182)
R_{free} (no. of *hkl* reflections)	0.255 (802)	0.294 (1142)	0.299 (695)	0.305 (926)
B factor (no. of atoms)				
protein	40.4 (1183)	66.6 (4750)	64.5 (4773)	57.9 (4413)
solvent/ligand	44.9 (92)	68.9 (2)	63.9 (1)	48.2 (6)
Ramachandran plot				
allowed (%)	97.1	97.2	95.6	96.9
generous (%)	2.2	1.7	2.4	1.7
disallowed (%)	0.7	1.1	2.0	1.4
root-mean-square deviation				
bonds (Å)	0.010	0.014	0.018	0.018
angles (deg)	1.31	1.64	2.06	1.84
PDB entry	3L9Z	3NXZ	3NY0	3LA0

[a] $R_{sym} = (\sum|I_{obs} - I_{avg}|)/\sum I_{avg}$. [b] $R_{work} = (\sum|F_{obs} - F_{calc}|)/\sum F_{obs}$.

RESULTS AND DISCUSSION

Initially purified *Hp*UreE protein was analyzed by mass spectrometry. While the expected molecular mass of UreE is 19381.5 Da, we observed two species with apparent masses of 18335 and 18149 Da. Because in the apo crystal structure all N-terminal residues, including the first methionine, are clearly visible in the electron density map while the C-terminus is disordered, this truncation must have occurred at the C-terminus. The difference in mass is consistent with a truncation of 10 (18294 kDa) or 12 (18107 kDa) residues. The mass difference of ~41 Da between the expected and observed molecular masses may be due to tightly bound ions. The protein used to obtain Cu-*Hp*UreE and Ni-*Hp*UreE was purified in the presence of protease inhibitor cocktail and did not undergo proteolysis.

Structure of the HpUreE Monomer. Each monomer of *Hp*UreE is composed of two domains. The N-terminal domain containing residues Met1−Asp77 adopts a four-stranded, mixed β-sheet with a long extension between strands β2 and β3 forming a β-hairpin with its strands nearly perpendicular to the main β-sheet (Figure 1a). The C-terminal domain, containing residues Ser78−Ser149, forms a five-stranded antiparallel β-sheet flanked on one side by two α-helices parallel to the strands.

The structure of the *Hp*UreE monomer is very similar to that of the *Ka*UreE monomers (*18*) and *Bp*UreE (*19*) monomers, which are 21.5 and 29.3% identical in sequence with *Hp*UreE, respectively. For example, the root-mean-square deviation (rmsd) for the 132 corresponding Cα atoms between *Hp*UreE and *Bp*UreE (PDB entry 1EB0) is 2.54 Å. However, the rmsd for the N-terminal (70 Cα atoms) or C-terminal domain (65 Cα atoms) is significantly smaller, 1.53 and 1.51 Å, respectively, indicating small differences in relative domain orientations in these two proteins.

Pairwise superposition of *Hp*UreE molecules from different crystal forms shows that while there are no significant structural differences among the N- and C-terminal domains, their relative disposition varies somewhat. Apo-*Hp*UreE differs the most from the other copies, with the bending around the interdomain linker leading to a translation of the residues furthest from the linker of as much as ~6.5 Å (Figure 1a).

Oligomeric Organization of HpUreE. We observed dimers or tetramers in the crystal structures that were formed in the absence or presence of UreE-bound metal ions, respectively. In the absence of metal ions, only dimers were observed (Figure 1b). This is in agreement with similar dimers observed in *Ka*UreE crystallized without added metals (*18*). In the presence of a metal ion, *Hp*UreE crystallized as a tetramer, with a dimer of dimers assembled around the metal ion (Figure 1c). We have obtained several tetragonal crystal forms of *Hp*UreE. We have confirmed that one of them contained Ni^{2+} (Ni-*Hp*UreE) and another Cu^{2+} (Cu-*Hp*UreE), while the identity of the metal in the third form was not identified directly (Me-*Hp*UreE). This metal is likely Zn^{2+}, Ni^{2+}, or Cu^{2+}. In all cases, the metal is coordinated by four $NE2^{His102}$ atoms located in a central plane (Figure 1d). Two water molecules are expected in apical positions to complete the octahedral coordination but are not always distinguishable because of limited resolution.

Inspection of the environment of His102 suggests that in the apo-*Hp*UreE form the side chain of His102 is likely oriented with its NE2 atom toward the main chain carbonyl of Asn100 from the other subunit in the dimer forming a hydrogen bond. For binding of the metal, the His102 side chain would have to rotate by 180° around the CB−CG axis, turning the NE2 atom toward the metal.

Previous characterization of Ni^{2+} and Zn^{2+} binding to *Hp*UreE by ITC indicates that only one Ni^{2+} binds per dimer and that the former involves His102 while the latter involves His102 and His152 (*4*). In our Me-*Hp*UreE and Cu-*Hp*UreE tetramer structures, His152 is within the disordered C-terminal segment. However, in the Ni-*Hp*UreE structure, the C-terminal segment of one of the four monomers is better ordered and His152 can be located reaching toward the Ni^{2+} ion, replacing one coordinating water molecule as a ligand (Figure 1e). This confirms that in

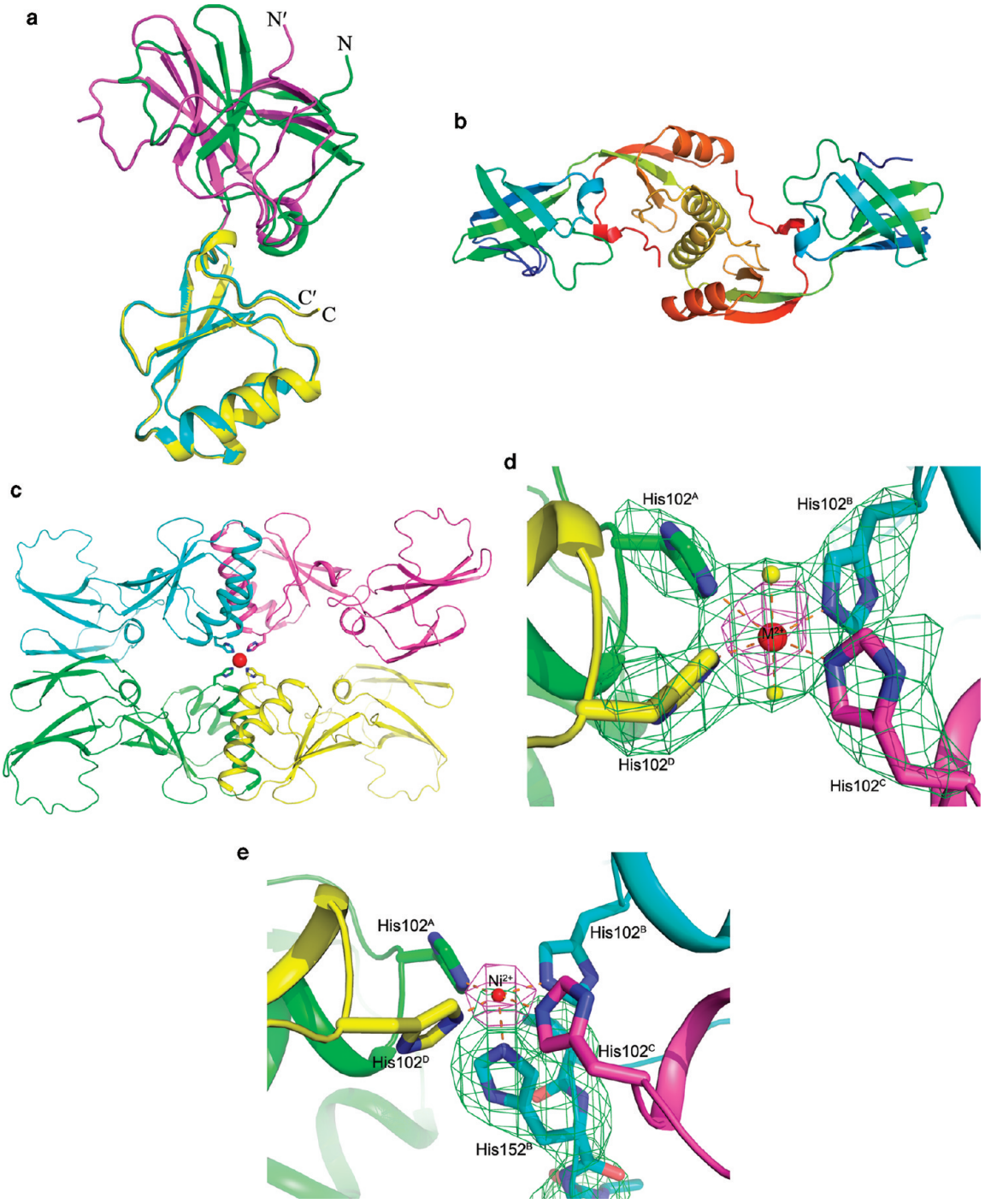

FIGURE 1: Structural details of UreE. (a) Superposition of the C-terminal domains of *Hp*UreE from apo-UreE (N-terminal domain colored green and C-terminal domain yellow) and Me-*Hp*UreE (N-terminal domain colored magenta and C-terminal domain cyan) showing a significant interdomain rotation. The molecules are shown in cartoon representation. (b) Dimeric form of apo-UreE with each subunit rainbow-colored (N-terminus colored blue and C-terminus red). (c) Crystal structure of Cu-UreE. The molecules form tetramers. (d) Coordination sphere of the Me^{2+} ion in Me-*Hp*UreE. The omit map (green) is contoured at 2.5σ with the metal ion (red sphere), two water molecules (yellow spheres), and the side chains of four histidine residues omitted from the calculation. The anomalous map (magenta; 0.9793 Å) contoured at 6σ is superimposed on the structure. The interactions between the coordinating elements and the metal ion are indicated by orange dashed lines. (e) Coordination of the Ni^{2+} ion in Ni-*Hp*UreE. His152 is ordered in only one of the four monomers. The omit map covering His152 is colored green and contoured at 3.5σ, and the anomalous map (magenta; 1.4849 Å) is contoured at 20σ.

solution the C-terminal histidine(s) can reach toward the central metal ion. There are two contacts between the dimers in the tetramer: (1) coordination around the central metal ion provided by His102 from all four subunits and (2) limited interactions between the N-terminal subunits involving a herringbone arrangement of Phe28 residues from two subunits. While a tetrameric arrangement was also observed in the crystal structure of *Bp*UreE, the relative orientation of the two dimers differs between the structures and depends on the coordination of the metal ion, which adopts either octahedral [our structure and type I *Bp*UreE (*19*)] or tetrahedral geometry [type II *Bp*UreE (*19*)].

Comparison with Other UreE Structures. Several metal ion-binding sites have been reported for *Ka*UreE and *Bp*UreE. Six Ni^{2+} ions per homodimer were initially reported for the

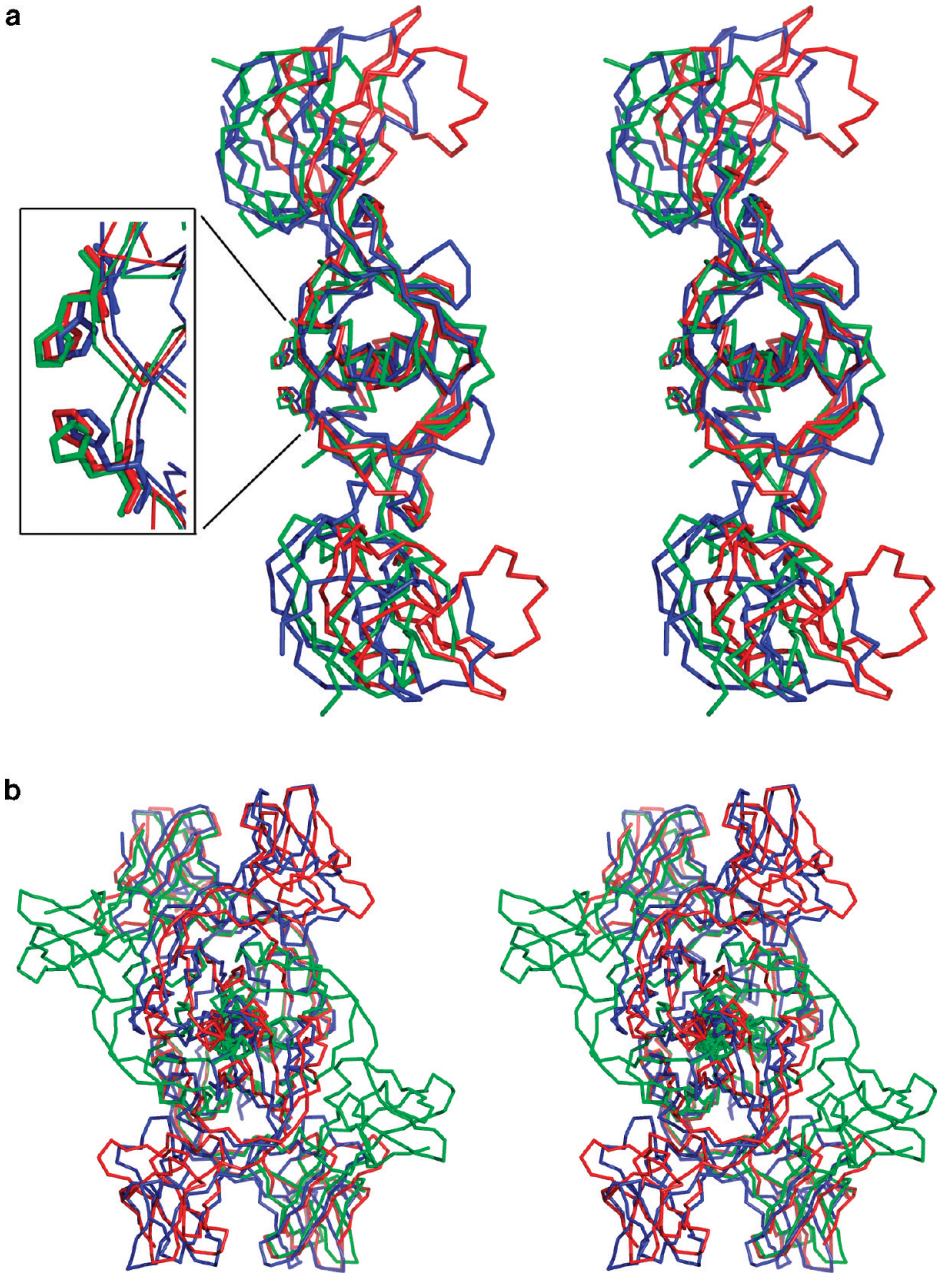

FIGURE 2: Superposition of UreE from different species. (a) Dimers of *Hp*UreE (blue), *Bp*UreE (red), and *Ka*UreE (green) superimposed on the basis of the C-terminal domains that form the dimer interface. The metal-liganding histidines are shown in stick mode, and a close-up is shown in the inset. (b) Superposition of tetramers of *Hp*UreE (blue), type I *Bp*UreE (red, PDB entry 1EB0), and type II *Bp*UreE (green, PDB entry 1EAR). The metal coordination in *Hp*UreE and type I *Bp*UreE is octahedral, while it is tetrahedral in type II *Bp*UreE.

full-length *Ka*UreE protein (*10*), and a truncated version (H144*UreE) lacking the histidine-rich C-terminal tail was shown to bind only two Ni^{2+} ions per dimer in solution (*30*). Analysis of the crystal structure of truncated H144*KaUreE revealed three Cu^{2+}-binding sites per dimer (*18*). The crystal structure of *Bp*UreE showed one metal ion (Zn^{2+}) bound to a tetramer (*19*), while analysis of purified *Bp*UreE by ICP-OES indicated that the protein could bind two Ni^{2+} ions per dimer (*15*); this is in contrast with findings from another group, whose NMR and equilibrium dialysis results suggest that the Ni^{2+} binding stoichiometry of *Bp*UreE is three Ni^{2+} ions per dimer, with the C-terminus of the protein involved in Ni^{2+} binding (*20*). The four C-terminal residues (including two histidines) were disordered in the *Bp*UreE crystal structure. The biological role of these multiple metal binding sites and the question of which of these are associated with transfer of the metal ion directly to the partner protein (presumably the apo-urease in *H. pylori*) are still unknown. Comparison of the UreE structures from three bacteria shows that the only common metal binding site between them is the one that is coordinated by His102 in *H. pylori* and the equivalent histidines in the two other structures (Figure 2a). The additional metal binding site (Cu^{2+} ion) observed in *Ka*UreE is formed by two histidines that are not conserved in other UreE sequences and are structurally equivalent mainly to Tyr/Phe and Lys residues in the other structures. The flexible C-termini are present in most UreE sequences and contain at least one histidine, while some (e.g., *Ka*UreE) contain several histidines in this segment (*16*). It was previously suggested that in *Hp*UreE, His152 located in the C-terminal tail helps to discriminate between Ni^{2+} and Zn^{2+} ions (*4*). Superposition of the structures

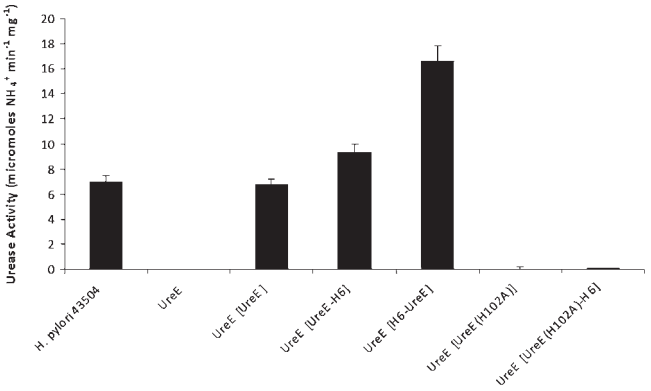

FIGURE 3: Urease activity of *H. pylori* 43504 and *ureE* mutants expressing different UreE variants. Constructs introduced by homologous recombination within the *hp0405* gene region of the *ureE* mutant are indicated. Results shown are the averages of assays conducted in triplicate; error bars denote standard deviations.

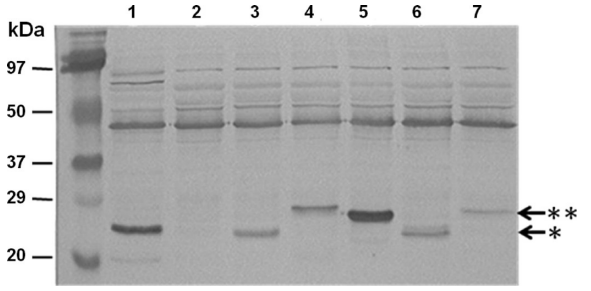

FIGURE 4: Immunoblotting against *H. pylori* UreE to compare levels of UreE expressed across tested strains: *H. pylori* 43504 (lane 1), *ureE* (lane 2), *ureE* [UreE] (lane 3), *ureE* [UreE-H6] (lane 4), *ureE* [H6-UreE] (lane 5), *ureE* [UreE(H102A)] (lane 6), and *ureE* [UreE(H102A)-H6] (lane 7). Arrows indicate UreE (one asterisk) or UreE containing a hexahistidine tag at either the C- or N-terminus (two asterisks). The positions of molecular mass standards are indicated at the left.

of *Hp*UreE, *Ka*UreE, and *Bp*UreE based on their C-terminal interface-forming domains shows that while the central metal binding site is structurally preserved, the relative orientation of N- and C-terminal domains varies. The dimers differ also in the distribution of electrostatic potential. While the potential near the central metal binding site is always negative, the electrostatic potential differs elsewhere.

Role of His102, His-Rich Segments, and the Additional Metal-Binding Sites. His102 in *Hp*UreE (*4*) and the equivalent His100 in *Bp*UreE (*19*) have been shown to play a key role in metal binding by these proteins. In addition, the H96A mutation of an equivalent histidine in *Ka*UreE significantly reduced urease activity in bacteria harboring this mutant (*11*, *31*). Similarly, the H102K mutation in *Hp*UreE had a deleterious effect on Ni^{2+} and Zn^{2+} binding, based on ITC analysis of this mutant (*4*). To explore the role of His102 further, we constructed a H102A mutant protein and expressed it in an *ureE*$^-$ background. Our controls included the *ureE* mutant as well as the 43504 parental strains. Urease assays were performed (Figure 3), and immunoblotting with anti-UreE antiserum was conducted to ensure that the UreE variants were expressed in each strain (Figure 4). The expression of *Hp*UreE(H102A) in the *ureE* mutant did not restore urease activity, indicating that the His102 residue of UreE is essential for the urease maturation process.

Many UreE sequences contain His-rich segments, usually in the C-terminal tail, and appear to bind multiple metal ions (*16*). We have previously shown that attachment of His-rich sequences to the C-terminus of *Hp*UreE leads to an elevated level of urease activity in *H. pylori hypA* or *hypB* mutants (*13*). The same effect is observed when the C-terminally hexahistidine-tagged *Hp*UreE is expressed in the *ureE*$^-$ (Figure 3) mutant strain. Therefore, we investigated the role of these His-rich segments in the function of UreEs. First, we inquired if the position of this segment at the C-terminus is essential for increased metal transfer activity. We expressed *Hp*UreE with a hexahistidine tag on the N-terminus and observed an even stronger effect on urease activity (Figure 3). Immunoblotting results indicated that the (N-terminal) His_6-*Hp*UreE was produced at greater levels than all other UreE variants (Figure 4, lane 5), and the higher urease activity seen in the *ureE* [H6-UreE] strain could be only partially attributed to the presence of the hexahistidine tag. Nevertheless, the addition of a His-rich segment to *Hp*UreE augmented urease activity, indicating a higher efficiency of Ni^{2+} transfer. The His-rich sequences found in some UreE proteins are known to sequester more Ni^{2+} ions (*13*, *32*), and the question of whether Ni^{2+} transfer can occur directly from the His-rich segments or must occur via coordination to His102 (or its equivalent) first arises. To answer this question, we introduced an H102A mutation into the UreE-His_6 construct and expressed it in an *ureE*$^-$ background. This strain had no urease activity, paralleling the behavior of the *ureE* [UreE(H102A)] strain (Figure 3). Therefore, our results clearly show that the metallochaperone activity of UreE is augmented by the presence of a pool of metal ions in the vicinity of the protein but that the transfer of Ni^{2+} ion must occur via coordination with His102; the His-rich regions would aid in the transfer by increasing the local effective concentration of available metal ions to replace the one transferred to a partner. The *Hp*UreE N-terminus is ~40 Å from the Ni^{2+} ion, while the last ordered C-terminal residue, Ser149, is ~16 Å from this ion. However, in one of the four monomers of Ni-*Hp*UreE, residues up to position 154 are clearly visible, with His152 folding back toward the Ni^{2+} ion.

In the presence of a metal ion, the *Hp*UreE molecules form tetramers in the crystal, with His102 coordinating the ion and only Phe28 from two different dimers in van der Waals contacts. The very limited contacts between the two dimers leave doubts about the physiological relevance of UreE tetramers, in particular since previously only dimers have been observed in solution by SEC, MALS/QELS light scattering, and TROSY-HSQC NMR experiments (*4*, *13*). To test the functional importance of tetramer formation, we expressed and purified an *Hp*UreE F28D mutant version. This replacement of a phenylalanine with an aspartate should introduce electrostatic repulsion between the dimers, significantly decreasing the likelihood of their association. Gel filtration showed that this protein forms dimers in solution in the presence or absence of metal ions. To investigate whether the Phe28 residue of UreE affected the in vivo activation of urease, the UreE(F28D) protein was expressed in the *ureE* mutant. The urease activity in this mutant was the same as in the complementary *ureE* [UreE] mutant strain (data not shown). Together, our data support previous conclusions that the tetramers observed in the crystals likely have little physiological significance and that the active form of *Hp*UreE is a dimer.

Interestingly, UreE tetramers (dimers of dimers or "kissing" dimers) associated via the metal ion have been observed also in *Bp*UreE (*17*, *19*) or *Ka*UreE (*14*). However, the relative orientation of the dimers within the tetramers varies, with the common feature being the coordination of the central metal ion by four histidines, equivalent to His102 in *Hp*UreE (Figure 2b). This

second occurrence of kissing dimers in *Hp*UreE crystals in the presence of metal ions suggests a mechanism for Ni^{2+} transfer. The kissing dimers with Ni^{2+} captured between them may mimic the interaction between a Ni^{2+}-loaded UreE dimer and the large subunit of apo-urease sharing the metal ion. The Ni^{2+} center in urease is surrounded by histidine side chains and is partially covered by a single loop [Val308−Pro343 in *H. pylori* urease (PDB entry 1E9Z)]. We hypothesize that this loop moves aside to allow the approach of UreE and that the Ni^{2+} presented by the UreE dimer can then be transferred to the urease histidine residues near the surface and subsequently move deeper into the urease active site, involving further coordination by additional histidines. Removal of the metal ion from the UreE−urease interface would then lead to release and departure of UreE.

ACKNOWLEDGMENT

We thank Shaunivan Labiuk [Canadian Light Source (CLS)] for collecting several data sets. Data for this study were collected at the Lilly Research Laboratory Collaborative Access Team (LRL-CAT) beamline at the Advanced Photon Source, Argonne National Laboratory, and at CMCF1 at CLS. Use of the Advanced Photon Source at Argonne National Laboratory was supported by the U.S. Department of Energy, Office of Science and Office of Basic Energy Sciences, under Contract DE-AC02-06CH11357. Use of the LRL-CAT beamline facilities at Sector 31 of the Advanced Photon Source was provided by Eli Lilly & Co. which operates the facility. The CMCF is supported by CFI, NSERC, and CIHR. This is NRCC publication 53123.

REFERENCES

1. Carter, E. L., Flugga, N., Boer, J. L., Mulrooney, S. B., and Hausinger, R. P. (2009) Interplay of metal ions and urease. *Metallomics 1*, 207–221.
2. Mulrooney, S. B., and Hausinger, R. P. (2003) Nickel uptake and utilization by microorganisms. *FEMS Microbiol. Rev. 27*, 239–261.
3. Heimer, S. R., and Mobley, H. L. T. (2001) Interaction of proteus mirabilis urease apoenzyme and accessory proteins identified with yeast two-hybrid technology. *J. Bacteriol. 183*, 1423–1433.
4. Bellucci, M., Zambelli, B., Musiani, F., Turano, P., and Ciurli, S. (2009) Helicobacter pylori UreE, a urease accessory protein: specific Ni(2+)- and Zn(2+)-binding properties and interaction with its cognate UreG. *Biochem. J. 422*, 91–100.
5. Voland, P., Weeks, D. L., Marcus, E. A., Prinz, C., Sachs, G., and Scott, D. (2003) Interactions among the seven Helicobacter pylori proteins encoded by the urease gene cluster. *Am. J. Physiol. 284*, G96–G106.
6. Stingl, K., Schauer, K., Ecobichon, C., Labigne, A., Lenormand, P., Rousselle, J. C., Namane, A., and de Reuse, H. (2008) In vivo interactome of Helicobacter pylori urease revealed by tandem affinity purification. *Mol. Cell. Proteomics 7*, 2429–2441.
7. Olson, J. W., Mehta, N. S., and Maier, R. J. (2001) Requirement of nickel metabolism proteins HypA and HypB for full activity of both hydrogenase and urease in Helicobacter pylori. *Mol. Microbiol. 39*, 176–182.
8. Mehta, N., Olson, J. W., and Maier, R. J. (2003) Characterization of Helicobacter pylori nickel metabolism accessory proteins needed for maturation of both urease and hydrogenase. *J. Bacteriol. 185*, 726–734.
9. Benoit, S. L., Zbell, A. L., and Maier, R. J. (2007) Nickel enzyme maturation in Helicobacter hepaticus: roles of accessory proteins in hydrogenase and urease activities. *Microbiology 153*, 3748–3756.
10. Lee, M. H., Pankratz, H. S., Wang, S., Scott, R. A., Finnegan, M. G., Johnson, M. K., Ippolito, J. A., Christianson, D. W., and Hausinger, R. P. (1993) Purification and characterization of Klebsiella aerogenes UreE protein: a nickel-binding protein that functions in urease metallocenter assembly. *Protein Sci. 2*, 1042–1052.
11. Colpas, G. J., Brayman, T. G., Ming, L. J., and Hausinger, R. P. (1999) Identification of metal-binding residues in the klebsiella aerogenes urease nickel metallochaperone, UreE. *Biochemistry 38*, 4078–4088.
12. Soriano, A., Colpas, G. J., and Hausinger, R. P. (2000) UreE stimulation of GTP-dependent urease activation in the UreD-UreF-UreG-urease apoprotein complex. *Biochemistry 39*, 12435–12440.
13. Benoit, S., and Maier, R. J. (2003) Dependence of Helicobacter pylori urease activity on the nickel-sequestering ability of the UreE accessory protein. *J. Bacteriol. 185*, 4787–4795.
14. Grossoehme, N. E., Mulrooney, S. B., Hausinger, R. P., and Wilcox, D. E. (2007) Thermodynamics of Ni^{2+}, Cu^{2+}, and Zn^{2+} binding to the urease metallochaperone UreE. *Biochemistry 46*, 10506–10516.
15. Stola, M., Musiani, F., Mangani, S., Turano, P., Safarov, N., Zambelli, B., and Ciurli, S. (2006) The nickel site of Bacillus pasteurii UreE, a urease metallo-chaperone, as revealed by metal-binding studies and X-ray absorption spectroscopy. *Biochemistry 45*, 6495–6509.
16. Musiani, F., Zambelli, B., Stola, M., and Ciurli, S. (2004) Nickel trafficking: insights into the fold and function of UreE, a urease metallochaperone. *J. Inorg. Biochem. 98*, 803–813.
17. Ciurli, S., Safarov, N., Miletti, S., Dikiy, A., Christensen, S. K., Kornetzky, K., Bryant, D. A., Vandenberghe, I., Devreese, B., Samyn, B., Remaut, H., and Van Beeumen, J. (2002) Molecular characterization of Bacillus pasteurii UreE, a metal-binding chaperone for the assembly of the urease active site. *J. Biol. Inorg. Chem. 7*, 623–631.
18. Song, H. K., Mulrooney, S. B., Huber, R., and Hausinger, R. P. (2001) Crystal structure of Klebsiella aerogenes UreE, a nickel-binding metallochaperone for urease activation. *J. Biol. Chem. 276*, 49359–49364.
19. Remaut, H., Safarov, N., Ciurli, S., and Van Beeumen, J. (2001) Structural basis for Ni^{2+} transport and assembly of the urease active site by the metallochaperone UreE from Bacillus pasteurii. *J. Biol. Chem. 276*, 49365–49370.
20. Won, H. S., Lee, Y. H., Kim, J. H., Shin, I. S., Lee, M. H., and Lee, B. J. (2004) Structural characterization of the nickel-binding properties of Bacillus pasteurii urease accessory protein (Ure)E in solution. *J. Biol. Chem. 279*, 17466–17472.
21. Ho, S. N., Hunt, H. D., Horton, R. M., Pullen, J. K., and Pease, L. R. (1989) Site-directed mutagenesis by overlap extension using the polymerase chain reaction. *Gene 77*, 51–59.
22. Weatherburn, M. W. (1968) Phenol-hypochlorite reaction for determination of ammonia. *Anal. Chem. 39*, 17466–17472.
23. Towbin, H., Staehelin, T., and Gordon, J. (1979) Electrophoretic transfer of proteins from polyacrylamide gels to nitrocellulose sheets: procedure and some applications. *Proc. Natl. Acad. Sci U. S. A. 76*, 4350–4354.
24. Blake, M. S., Johnston, K. H., Russell-Jones, G. J., and Gotschlich, E. C. (1984) A rapid, sensitive method for detection of alkaline phosphatase-conjugated anti-antibody on Western blots. *Anal. Biochem. 136*, 175–179.
25. Benoit, S. L., Mehta, N., Weinberg, M. V., Maier, C., and Maier, R. J. (2007) Interaction between the Helicobacter pylori accessory proteins HypA and UreE is needed for urease maturation. *Microbiology 153*, 1474–1482.
26. Otwinowski, Z., and Minor, W. (1997) Processing of X-ray diffraction data collected in oscillation mode. *Methods Enzymol. 276*, 307–326.
27. McCoy, A. J., Grosse-Kunstleve, R. W., Adams, P. D., Winn, M. D., Storoni, L. C., and Read, R. J. (2007) Phaser crystallographic software. *J. Appl. Crystallogr. 40*, 658–674.
28. Emsley, P., and Cowtan, K. (2004) Coot: model-building tools for molecular graphics. *Acta Crystallogr. D60*, 2126–2132.
29. Murshudov, G. N., Vagin, A. A., Lebedev, A., Wilson, K. S., and Dodson, E. J. (1999) Efficient anisotropic refinement of macromolecular structures using FFT. *Acta Crystallogr. D Biol. Crystallogr. 55*, 247–255.
30. Brayman, T. G., and Hausinger, R. P. (1996) Purification, characterization, and functional analysis of a truncated Klebsiella aerogenes UreE urease accessory protein lacking the histidine-rich carboxyl terminus. *J. Bacteriol. 178*, 5410–5416.
31. Colpas, G. J., and Hausinger, R. P. (2000) In vivo and in vitro kinetics of metal transfer by the Klebsiella aerogenes urease nickel metallochaperone, UreE. *J. Biol. Chem. 275*, 10731–10737.
32. Maier, R. J., Benoit, S. L., and Seshadri, S. (2007) Nickel-binding and accessory proteins facilitating Ni-enzyme maturation in Helicobacter pylori. *Biometals 20*, 655–664.